Smith, Jason M and Grazioso, Fabio and Patton, Brian R and Dolan, Philip R and Markham, Matthew L and Twitchen, Daniel J (2011) Optical properties of a single-colour centre in diamond with a green zero-phonon line. New Journal of Physics, 13. ISSN 1367-2630 , http://dx.doi.org/10.1088/1367-2630/13/4/045005

This version is available at https://strathprints.strath.ac.uk/60677/

Optical properties of a single-colour centre in diamond with a green zero-phonon line

Jason M Smith[1,3]**, Fabio Grazioso**[1]**, Brian R Patton**[1]**,
Philip R Dolan**[1]**, Matthew L Markham**[2] **and Daniel J Twitchen**[2]

[1] Department of Materials, University of Oxford, Parks Road,
Oxford OX1 3PH, UK
[2] Element Six Ltd, Kings Ride Park, Ascot, Berkshire, SL5 8BP, UK
E-mail: jason.smith@materials.ox.ac.uk

Abstract. We report the photoluminescence characteristics of a colour centre in diamond grown by plasma-assisted chemical vapour deposition. The colour centre emits with a sharp zero-phonon line at $2.330\,\text{eV}$ ($\lambda = 532\,\text{nm}$) and a lifetime of $3.3\,\text{ns}$, thus offering potential for a high-speed single-photon source with green emission. It displays a vibronic emission spectrum with a Huang–Rhys parameter of 2.48 at $77\,\text{K}$. Hanbury–Brown and Twiss measurements reveal that the electronic level structure of the defect includes a metastable state that can be populated from the optically excited state.

---

[3] Author to whom any correspondence should be addressed.

IOP Institute of Physics Φ DEUTSCHE PHYSIKALISCHE GESELLSCHAFT

Contents

1. Introduction

Spectroscopic study of diamonds over the past 50 years or so has revealed hundreds of different emission lines, and the origin of the vast majority of these has not yet been positively identified [1]. In the past 10 years, a great deal of focus has been turned to the nitrogen-vacancy (NV) defect, especially in its negatively charged state, NV^-. Detailed study of this particular defect has been facilitated in large part because isolated NV centres are readily found in both natural and synthetic diamonds, and because they show sufficient photostability to allow many controlled experiments to be performed on single emitters. The NV centre is now well established as a room-temperature single-photon source [2][4], and is competitive with other technologies as a physical spin qubit for quantum computing [3]–[7].

There are, however, aspects of the physics of NV^- that are (at least) inconvenient in the pursuit of these applications, one of which is the strongly vibronic nature of the optical transition, quantified by a Huang–Rhys factor of 3.2 at low temperature. The result is a broad emission spectrum that is not ideal for quantum communications, with only 4% of the photons emitted into the zero-phonon line (ZPL) at 637 nm. The low probability of ZPL emission presents specific challenges for some processes, such as entanglement-by-measurement in which only ZPL photons can be used [6].

This and other apparent drawbacks of NV^- may not ultimately prevent its use in advanced quantum applications, particularly if some control can be exercised over the emission properties, for example, by employing suitable optical cavities [8, 9], but they at least provide a motivation for identifying other colour centres in diamond that may eventually supersede it in some application areas. At the time of writing this search is at an early stage and is limited to a few recent reports of the silicon-vacancy (SiV) centre [10, 11] and nickel [12, 13] and chromium-related colour centres [14, 15], plus an intense two-level centre that is yet to be identified [16]. These centres show promise as single-photon sources for quantum key distribution, due to much weaker phonon coupling, but the extent to which they may be useful for wider quantum

---

[4] A commercially available single-photon source based on diamond NV centres can be found at www.qcvictoria.com

technologies is at present unclear. It is therefore important to identify new colour centres with potential for use in these application areas.

In this paper, we present a spectroscopic study of a single-colour centre with the principal ZPL at 2.330 eV (532 nm), found in high-purity diamond grown by chemical vapour deposition (CVD). A line very close to this energy is observed routinely in less pure CVD-grown diamond, and some of its properties have been documented in several reports [17]–[22], but it has not previously been studied as a single centre. Its physical structure is yet to be identified, although it is thought to relate to a nitrogen or boron complex and it has been suggested that it may have C_{3v} symmetry [1] (an attribution that is called into question here). With the additional specificity of single-centre spectroscopy and the information present in photon emission statistics, we are able to characterize the colour centre in significantly more detail than has been hitherto achieved. We show that its luminescence signature has similarities to that of NV^-, but with weaker phonon coupling and a shorter excited state lifetime, indicating potential for its use in quantum photonics applications.

2. Experimental

The sample studied was a high purity, [001]-oriented type IIa diamond grown by microwave plasma-assisted CVD [23]. Homoepitaxial CVD diamond growth was performed using a selected high-pressure high-temperature-grown substrate, which had been carefully processed prior to growth in order to minimize the dislocation density in the grown CVD diamond. The resultant diamond had a nitrogen concentration of < 5 ppb, as measured by ensemble electron paramagnetic resonance (EPR), and a boron concentration of < 0.5 ppb, as measured by secondary ion mass spectrometry (SIMS). After growth, the sample was mechanically polished to have a surface root mean square roughness < 1 nm over a $1 \times 1\,\mu$m area.

Photoluminescence (PL) imaging and spectroscopy were performed using a custom-built scanning confocal microscope that allowed the sample to be cooled in a bath cryostat, the full design and specifications of which are reported elsewhere [24]. Excitation was performed using a frequency-doubled YAG laser ($\lambda = 532$ nm) with a maximum power delivery to the sample of 13 mW, and a PicoQuant GaInN diode laser ($\lambda = 473$ nm) that can be operated in both continuous wave (cw) and Q-switched modes, the latter delivering pulses of 100 ps duration. In cw mode up to 1.5 mW of power is delivered to the sample using this laser. Spectra were recorded with an Acton SpectraPro 0.75 m monochromator fitted with a Princeton Spec-10 100B back-illuminated CCD camera, with $> 90\%$ quantum efficiency across the wavelength range of interest.

An image of the sample viewed using white light transmission between crossed polarizers is shown in figure 1(a). Through most of the sample the concentration of colour centres is extremely low $< 10^8\,\text{cm}^{-3}$. Regions of high birefringence, corresponding to stress of order 1 GPa[5], can be seen towards the right-hand edge of the sample, and PL imaging of this region reveals a much higher density of colour centres, both individually and as ensembles that appear to decorate extended defects. Figures 1(b) and (c) show PL images of a $20 \times 20\,\mu$m region of the sample both under 532 and 473 nm excitations. In the former case, a 532 nm laser clean-up filter is used in excitation, combined with a 540 nm dichroic beam splitter and a 532 nm

---

[5] The magnitude of the local stress was measured by recording the splittings in the ZPLs of nearby negatively charged NV colour centres [25].
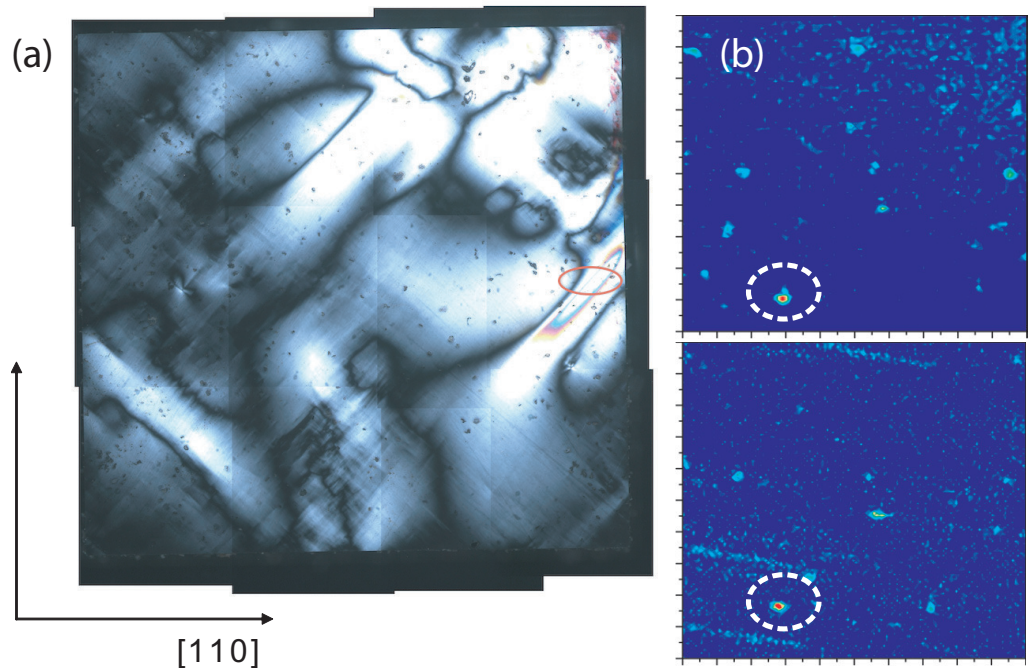
Figure 1. (a) Birefringence image of the CVD diamond sample viewed in white light transmission with the sample placed between crossed polarizers. The viewing axis is [001] and the sample edges are {110} crystal planes. The circled region near the middle of the right-hand edge shows particularly high stress, of order 1 GPa, that was present during growth; (b) false colour images of the photoluminescence (PL) intensity from a $20 \times 20\,\mu$m area of the sample in the high stress region under 532 nm (upper image), and 473 nm (lower image) excitation. The '532' colour centre is the brightest feature in both images, and is circled.

blocking notch filter in the collection optics. Under 473 nm excitation the filter set included a narrow band-pass clean-up filter in the excitation optics, a 500 nm dichroic beam splitter and an abrupt 510 nm long-pass filter in collection. In both images the '532' colour centre is circled. All data presented in this report were recorded from this one defect. The other defects observed are either NV$^-$ centres (visible under 532 nm excitation but not 473 nm) or other colour centres that are not photostable single emitters and are not considered further here.

3. Results and analysis

3.1. Photoluminescence (PL) spectroscopy

Figure 2(a) shows the PL spectrum of the 532 colour centre at 300 K (upper plot) and at 77 K (lower plot), under $\lambda = 473$ nm excitation. In the raw data (not shown) the second-order Raman signal from the bulk diamond was situated between 520 and 540 nm. By measuring the Raman independently from a region near to the colour centre and subtracting this data set we arrive at the pure luminescence signals shown in the figure. The spectra are dominated by a ZPL at 532 nm and associated phonon sidebands, with a second narrow line visible at 578 nm. The
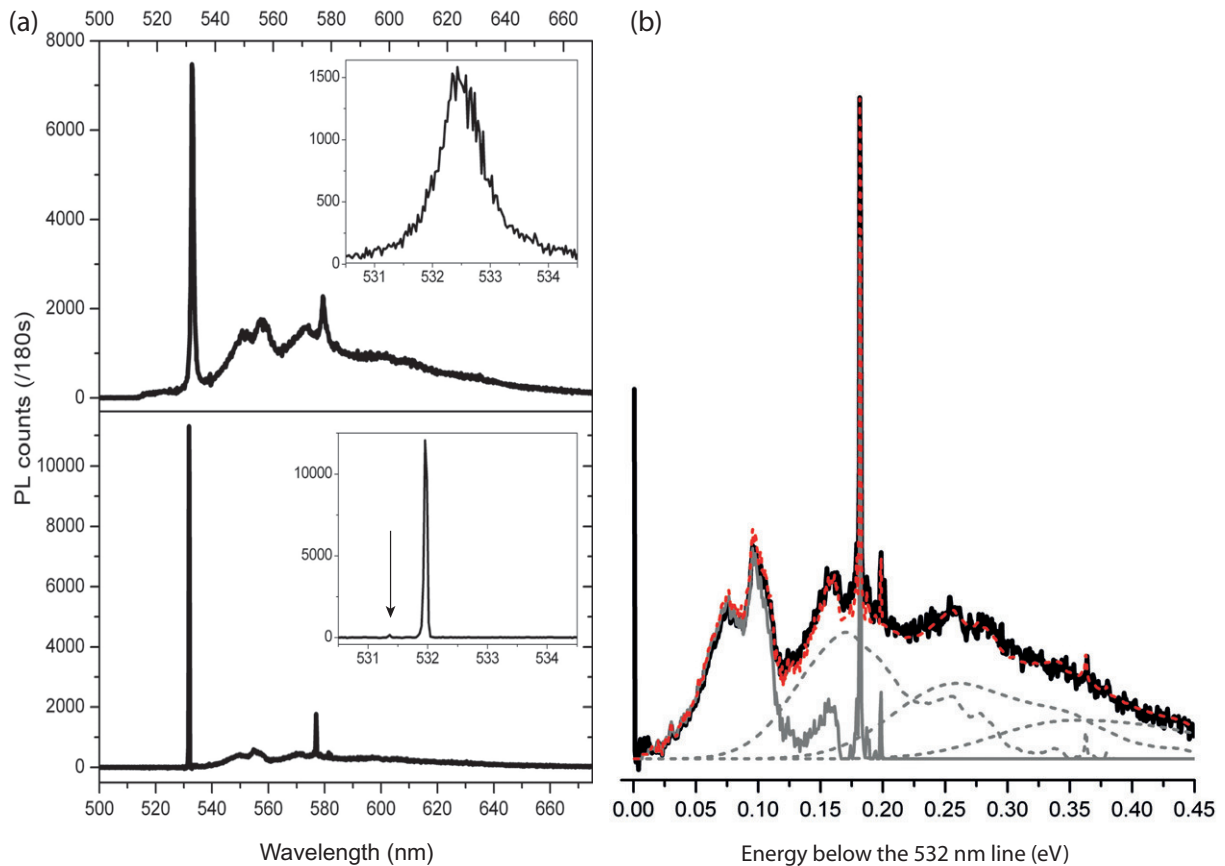
Figure 2. (a) PL spectra of the 532 centre under 473 nm excitation at 300 K (upper plots) and at 77 K (lower plots). The main figures show the full spectra and the insets show close-ups of the ZPL. (b) Analysis of the vibronic spectrum at 77 K. The red-dashed line is the sum of the contributions for up to four phonons emitted, obtained by repeated convolution of the one-phonon spectrum (solid grey line), with a Huang–Rhys factor of $S = 2.48$. The $n = 2$, 3 and 4 lineshapes calculated using equation (2) are shown as broken grey lines.

532 nm line comprises 10% of the emission intensity at 300 K and 12% of the intensity at 77 K. Both narrow lines are well resolved at room temperature with approximately Lorentzian lineshapes of width about 0.8 nm. From the 300 K spectrum it is clear that, referring back to the images in figure 1(b), the centre is excited resonantly with the frequency-doubled YAG and non-resonantly with the GaInN diode laser.

Close-ups of the 532 nm line at the two temperatures measured are shown in the insets to figure 2(a). On cooling to 77 K the line blue-shifts by 0.5 nm and narrows to a width of <0.05 nm, beyond the resolution of our spectrograph. Close inspection of the low-temperature ZPL spectrum reveals a second peak at 531.4 nm that is about 1% of the intensity of the main peak (marked by an arrow). The 578 nm line narrows in a fashion similar to the main 532 nm line upon cooling, but undergoes a smaller blue-shift of 0.2 nm.

By placing a linear optical polarizer alternately in the excitation path and the luminescence collection path of the microscope, we find that both in excitation and emission the colour centre

couples to light that is strongly ($>90\%$) linearly polarized parallel with the [110]-direction of the crystal. This is found to be true both for resonant and non-resonant excitations of the 532 nm line, and at both temperatures measured. The sharp lines at 532 and 578 nm are both co-polarized along this axis, as is the weaker line visible at 531.4 nm at 77 K, although in the latter case the weakness of the line means that the degree of polarization is less clear.

We model the emission spectrum that includes the 532 nm ZPL and its associated phonon sidebands following the method of Davies [26]. The initial state of the emission transition is assumed to be the lowest-energy ($n = 0$) vibrational eigenstate of the electronic excited state. Following the Franck–Condon principle, the probability of emission into the n-phonon vibrational level of the ground electronic state is then proportional to the square of the overlap integral between the initial and final vibrational eigenstates, which for a harmonic oscillator potential gives the standard result

$$|M_{0n}|^2 \propto \frac{S^n}{n!}, \tag{1}$$

where S is the Huang–Rhys factor. The lineshape for the transition involving the creation of n phonons, $I_n(E_v)$ is determined by $n-1$ convolutions of the single-phonon lineshape $I_1(E_v)$, where E_v is the vibrational energy of the lattice immediately after the optical transition:

$$I_n(E_v) = \int_{x=0}^{E_{max}} I_1(x) I_{n-1}(E_v - x) \, dx. \tag{2}$$

Here E_{max} is the maximum energy of the one-phonon distribution. The emission spectrum for the phonon sideband is given by the sum of these terms weighted by their Franck–Condon factors, multiplied by the photon density of states:

$$I(E) \propto E^3 \sum_{n=1}^{\infty} I_n(E_v) |M_{0n}|^2, \tag{3}$$

where E is the photon energy. Figure 2(b) shows the application of this theory to the measured 77 K data, plotting probability densities (i.e., intensity divided by E^3) as functions of the photon energy measured below the 532 nm line. The black solid line represents the measured data. The analysis was carried out as follows. From a first estimate of the single-phonon lineshape, equation (2) was used to calculate the lineshapes for the contributions from two- to four-phonon processes. The value of S was established from the fraction of the probability density that appears in the ZPL, as $S = -\ln(I_0)$. Equations (1)–(3) were then iterated, adjusting $I_1(E_v)$ until the best fit was obtained to the measured spectrum.

A Huang–Rhys factor of $S = 2.48$ combined with the single-phonon lineshape shown as the solid grey line in figure 2(b) produce the plotted contributions for up to four emitted phonons. The sum of these contributions is shown as the red-dashed line. The single-phonon lineshape required to give an accurate fit is a continuum up to the cut-off at 165 meV that represents the upper limit of the bulk phonon energies [27], within which range it is greatest at acoustic phonon energies between 50 and 110 meV and is split into a doublet. A small amount of coupling to bulk optical modes is visible around 150 meV. In addition, two sharp peaks are required at higher energies—a strong peak at 182 meV, and a weaker one at 199 meV—that are attributed to local vibrational modes that do not penetrate the surrounding bulk material. This single-phonon lineshape leads to an exceptional agreement between the calculated spectrum and the experimental data; for example, we note that the convolution of a localized 182 meV phonon
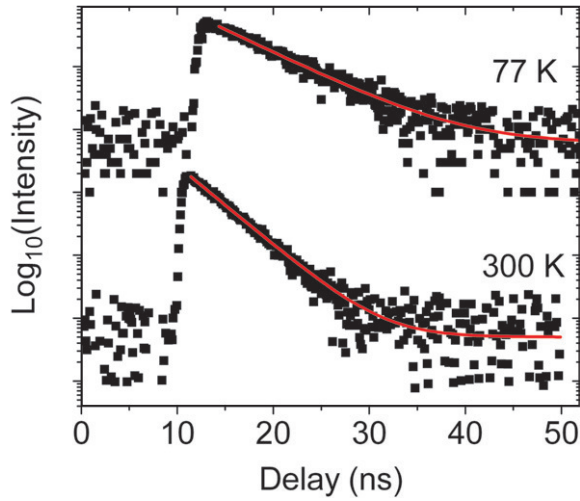
Figure 3. Semilogarithmic plot of the time-resolved PL for the 532 colour centre at 77 K (upper plot) and 300 K (lower plot). The data are corrected for background and shown as scatter graphs. Fits to single exponential decays are shown as solid red lines.

and a bulk acoustic phonon produces a doublet between 250 and 280 meV, while the emission of two localized phonons is visible as a small but sharp peak at 364 meV.

3.2. Time-resolved PL

The PL decay of the colour centre after pulsed excitation at 473 nm was measured at 300 K and 77 K using time-correlated single-photon counting. Both data sets, shown on semilogarithmic axes in figure 3, fit well to single exponential decay functions. The decay lifetime at 300 K is measured to be $\tau = 3.3 \pm 0.1$ ns, and at 77 K is measured to be $\tau = 5.9 \pm 0.3$ ns. These values have been verified with iterative reconvolution of the instrumental response function that has a full-width at half-maximum as FWHM = 0.7 ns resulting from the timing jitter of the detector.

The spontaneous emission rate of the centre is related to its transition dipole moment d by the equation

$$\frac{1}{\tau} = \frac{2 n_s e^2 \omega^3 |d|^2}{3 \epsilon_0 h c^3},$$

(4)

where n_s is the refractive index of the surrounding medium and ω is the transition angular frequency, giving $d = 2.6 \times 10^{-29}$ cm or 7.7 Debye at room temperature, dropping to 1.9×10^{-29} cm or 5.8 Debye at 77 K. The origin of such a significant temperature dependence to the decay dynamics is at present unclear, but it may suggest that the lifetime is determined in part by non-radiative relaxation that includes some phonon mediation and is therefore suppressed at low temperature.

3.3. Excitation power dependence

The ZPL linewidth is found to be unchanged as the $\lambda = 473$ nm excitation power is varied from 16 μW to 1.4 mW at 300 K, indicating that it is not influenced on the meV energy scale

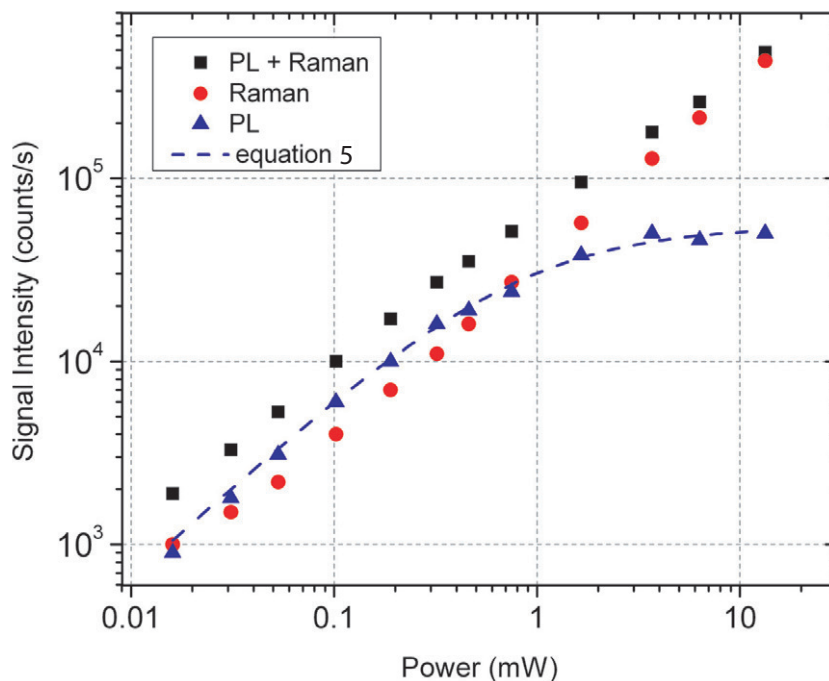**IOP** Institute of Physics Φ DEUTSCHE PHYSIKALISCHE GESELLSCHAFT

Figure 4. Saturation curves for the PL intensity from the 532 colour centre. The scatter graphs show the photon count rates measured aligned to the defect (squares), off the defect (circles) and the difference between the two (triangles) that represents only PL from the colour centre. The dashed line is the least squares fit of the saturation equation in the text to the PL intensity.

by spectral drift. Figure 4 shows logarithmic scatter graphs for the combined PL and Raman intensity measured with 532 nm excitation when aligned optimally to the colour centre, the Raman intensity aligned away from the colour centre, and the difference between the two signals (PL only). Note that to observe saturation of the emission it was necessary to exploit the higher-excitation power available from the 532 nm laser, which meant that both first- and second-order Raman signals contributed to the background, and limit the signal-to-background intensity ratio to about 2 : 1. When using the 532 nm excitation the spectrum of the detected emission was that of the vibronic side band from 540 to 700 nm, and was checked to ensure that no contribution from nearby NV centres was present. The saturation behaviour of the PL intensity from the colour centre can be observed clearly in the data, and is well fitted by the standard expression

$$I = \frac{F_0 P}{P + P_{\text{sat}}}, \tag{5}$$

where P is the excitation power, and F_0 and P_{sat} are constants. The dashed line in figure 4 follows the curve with $F_0 = 6 \times 10^4$ counts per second and $P_{\text{sat}} = 820 \pm 90\,\mu\text{W}$. In viewing the saturation power figure it should be noted that significant spherical aberrations are expected since the objective lens does not correct well for the planar diamond/air interface, resulting in a likely overestimate of the saturation intensity if a diffraction-limited spot is assumed. F_0, the saturation count rate, is limited by the quality of the objective lens used in the microscope, but is approximately 2.8 times that recorded from single NV$^-$ colour centres with the same optical
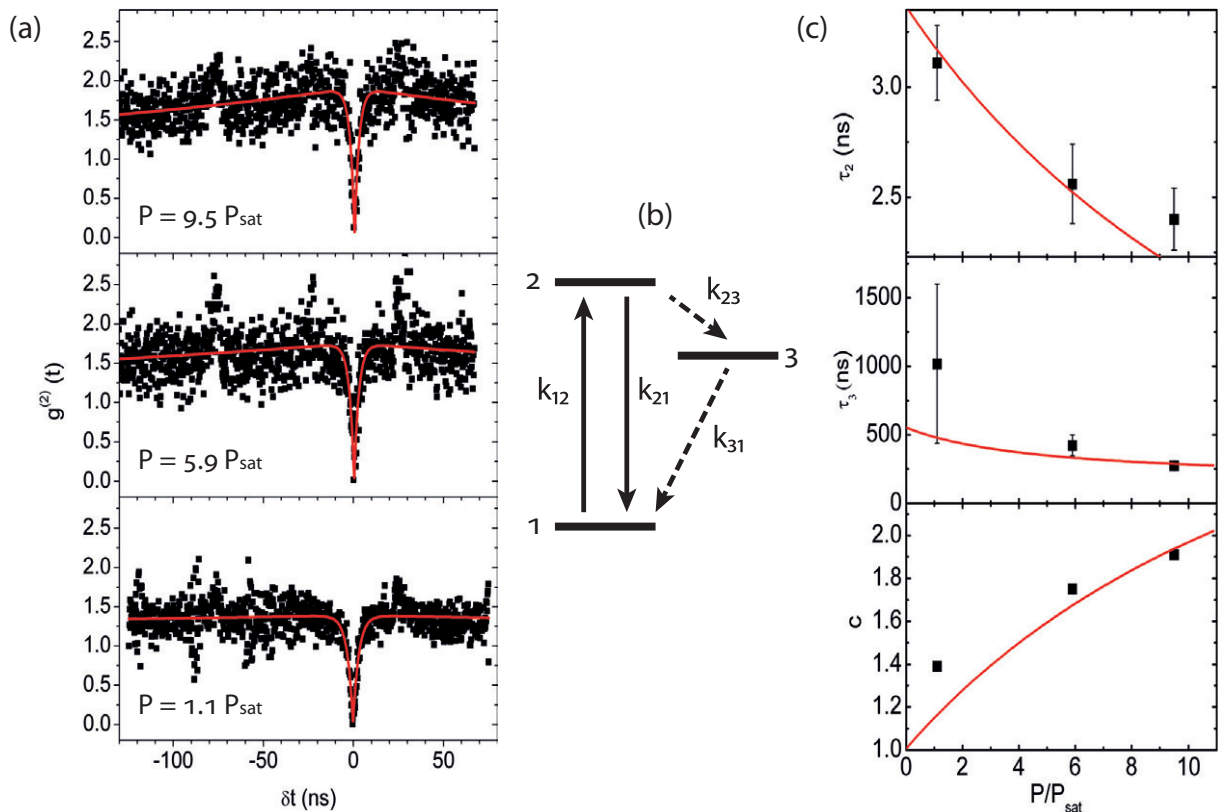
Figure 5. (a) Hanbury–Brown and Twiss measurements of the photon correlation function $g^{(2)}(\delta t)$ at excitation powers of 1.1, 5.9 and 9.5 times P_{sat}. The red lines are the best fits to equation (4). (b) The three-level system and rate constants used to model the $g^{(2)}$ data. Level 1 is the ground state, 2 is the optically excited state and 3 is the metastable state. Weaker transitions are indicated by dashed arrows. (c) Scatter graphs of the parameters τ_1, τ_2, and c against excitation power, and theoretical curves (solid lines) that follow equations (7)–(10) using the parameters given in the text.

apparatus [24], taking into account the slightly lower detection efficiency of the single-photon counter (Perkin Elmer SPCM AQR series) at the shorter emission wavelength.

3.4. Autocorrelation measurements

Hanbury–Brown and Twiss measurements of the photon autocorrelation function for the colour centre at 300 K were recorded with resonant 532 nm excitation of 0.9, 4.9 and 7.8 mW, and the results are shown as scatter graphs in figures 5(a). The datasets shown have been corrected for the measured Raman background by identification of the ratio of the signal to the background count rate, and using this to calculate the level of the autocorrelation counts involving at least one background photon as a fraction of the total autocorrelation counts as $\delta t \to \infty$. This background level is then subtracted. The resulting datasets in the figure show characteristic dips very close to zero at $\delta t = 0$. Note that the unavoidable presence of a substantial background in the autocorrelation measurements results in an increased level of noise in the data for a given

acquisition time. Normalization of the $g^{(2)}$ data was carried out by recognizing that $g^{(2)} = 1$ at long time delays in the limit of low excitation power, and then scaling with the square of the signal count rate at the higher-excitation powers. As with the saturation data in figure 4, the 532 nm laser was chosen here to provide excitation intensities $\gg P_{\text{sat}}$. Excitation using the 473 nm non-resonant source, with a maximum intensity of 1.5 mW, gave autocorrelation data very similar to the 0.9 mW data in the figure and are not shown.

The $g^{(2)}$ data for $P > P_{\text{sat}}$ show increasing signs of photon bunching at longer delay times, characteristic of a metastable state accessible from the optically excited state. We therefore use a three-level system to model the experimental results, shown in figure 5(b). Level 1 is the ground state, level 2 the optically excited state and level 3 the metastable state, with k_{ij} representing the incoherent transition rate from states i to j. Solving the coupled rate equations corresponding to the evolution of the probability distribution for occupation of each of these levels at time δt after initialization in level 1 (i.e. immediately after a photon emission event) results in the autocorrelation function

$$g^{(2)}(\delta t) = 1 - c e^{-|\delta t|/\tau_2} + (c-1)e^{-|\delta t|/\tau_3}, \tag{6}$$

where c, τ_2 and τ_3 are related to the inter-level rate constants by

$$\tau_{2,3} = \frac{2}{A \pm \sqrt{A^2 - 4B}}, \tag{7}$$

$$A = k_{12} + k_{21} + k_{23} + k_{31}, \tag{8}$$

$$B = k_{12}k_{23} + k_{12}k_{31} + k_{21}k_{31} + k_{23}k_{31}, \tag{9}$$

$$c = \frac{1 - \tau_2 k_{31}}{k_{31}(\tau_3 - \tau_2)}, \tag{10}$$

as described in [11]. The solid curves in figure 5(a) are least-squares fits of equation (6) to the measured data. The experimentally fitted parameters c, τ_2 and τ_3 are plotted as scatter graphs in figure 5(c), as functions of the excitation power normalized to P_{sat}. The solid red lines show the plots of the theoretical expressions from equations (7) and (10) using the values $k_{21} = 2.99 \times 10^8 \, \text{s}^{-1}$, $k_{23} = 3.8 \times 10^6 \, \text{s}^{-1}$ and $k_{31} = 1.4 \times 10^6 \, \text{s}^{-1}$. The fits demonstrate a reasonable agreement between theory and experiment, and particularly noteworthy is the very good agreement between the population decay rate of level 2 and the time-resolved PL lifetime of 3.3 ns reported in section 3.2. The error bars in the level 3 coupling rates are quite large, but agreement with the theoretical curves is sufficient to establish that at least one metastable level must be present, with a lifetime of order 1 μs.

3.5. Photostability

All of the data in this paper were recorded from the single-colour centre indicated in figure 1, demonstrating very good photostability for this colour centre. The observed signal intensity was free of any blinking or intensity fluctuations throughout the measurements. Ultimately, however, the PL signal stopped abruptly and permanently after about an hour of continuous excitation under 1.5 mW of 473 nm laser light. It is not currently clear what caused this change, but a photoionization process, perhaps catalysed by absorption of a second photon while in the excited state, appears most likely. Efforts are currently underway to see if the luminescent state can be restored by further optical pumping, and to investigate the photostability of other

similar centres. It is also possible the the local stress in the lattice plays a role. Nevertheless, the prolonged photostability of the measured colour centre prior to the photobleaching event is encouraging.

4. Discussion

To investigate the origin of this colour centre we compare our results with those presented previously. Burton *et al* [19], Kanda *et al* [20, 21] and Tallaire *et al* [22], all report CL spectra very similar to those in figure 2(a) above, in which a sharp ZPL in the vicinity of 532 nm is accompanied by a vibronic sideband with a first peak about 80 meV lower in energy, but in their (less pure) samples the remainder of the spectrum is obscured by strong emission from the neutral NV centre. The 533 nm ZPL observed in CL measurements has been reported both as a singlet and a doublet, and it has been argued that the line is split due to local strain [19]. The observed splitting of the ZPL doublet in figure 2(b) above is consistent with that in [19] given the respective strains present in the two samples. It is therefore possible that the centre reported here is the same as that in these reports. In earlier reports by Khong and Collins [17], and Khong *et al* [18], sharp CL features were observed at 532 nm in CVD diamond, which were found to increase in brightness at low temperature and displayed a luminescence lifetime of about 1 ns. We observe no strong intensity change with temperature, and a longer lifetime, but both these apparent discrepancies could be explained by environmental effects, and so a link between our data and those reported in [17] and [18] also remains possible.

The vibronic spectrum with coupling to continuum vibrational modes of the diamond lattice suggests a defect containing a low-mass impurity such as nitrogen or boron [26, 28], although the presence of higher-energy local vibrational modes in the emission spectrum may indicate the existence of an interstitial as a component of the defect [29]. The 533 nm line has been observed to be unstable under annealing at 1200 °C [30], providing a further clue as to its physical structure. A systematic study of the defect symmetry, for example, by application of uniaxial stress, is yet to be performed, and CL measurements on ensembles of the colour centre have recorded no optical polarization of the emission [31], and so little is known about the orientation of the optical transition dipoles. If the two lines observed in the 77 K ZPL spectrum in figure 2(a) are a stress-split orbital doublet, their dipoles should be orthogonal, and yet in our measurements the two lines appear similarly polarized. Clearly this situation could only occur if the viewing axes were coplanar with the two orthogonal dipoles, i.e. if the dipoles lay in the $(1\bar{1}0)$ plane. The relative weakness of the higher-energy transition of the doublet may then suggest that it is oriented more closely to the [001] viewing axis. Consideration of the geometrical optics [32] suggests that the degree of polarization observed for the weaker line could result, provided its angle to [001] is greater than about 15°. That these two lines correspond to a stress-split doublet is, however, only one of several possibilities, and more measurements are required to positively identify the dipole orientations and defect symmetry. We note that our data do allow us to exclude the possibility suggested in [1] that the two lines of the doublet result from degeneracy lifting in a C_{3v} colour centre under stress, since the planes normal to the C_{3v} axes are {111} in the cubic crystal, and orthogonal transition dipoles in this plane would necessarily make angles between 60° and 90° when projected on the (001) plane.

We conclude with a brief comparison between the properties of the 532 centre and those for the other single-colour centres in diamond that have been reported to date. Table 1 presents the ZPL energies and widths, Huang–Rhys factors, and fluorescence lifetimes, for the 532 centre,

Table 1. Table of parameters for the 532 centre, compared with those of the other diamond colour centre single-photon sources characterized to date.

Parameters	532	NV$^-$	SiV[a]	NE8	Cr[a]	U2LS[b]
ZPL energy (eV)	2.330	1.945	1.68	1.55	1.61–1.68	1.69
ZPL width at 300 K (nm)	0.8	2	0.7–4.9	2[c]	3–10	4.1
Huang–Rhys factor[d]	2.48	3.2	0.2	0.4	–	0.2
Lifetime (ns)	3.3	12.6	2	11.5	1–14	13.6

[a]The data reported for SiV and Cr defects vary considerably between centres, and so these figures should be taken only as representative.
[b]U2LS is the unidentified two-level system of [16].
[c] Value estimated from data presented in [12].
[d]The 532 and NV$^-$ centres Huang–Rhys parameters are low-temperature values, whereas SiV, NE8 and U2LS were reported at 300 K.

NV$^-$, SiV, Ne8 and Cr centre of references [14] and [15], and the unidentified two-level system (U2LS) of reference [16]. Perhaps the principal attraction of the 532 colour centre is its strong ZPL at a wavelength for which stable single-photon sources are scarce. The 0.8 nm ZPL width at room temperature is as narrow as any that have been observed from diamond colour centres, with only the SiV having shown comparably narrow ZPL emission. The Huang–Rhys factor of the 532 centre places it in a similar class to NV$^-$, with coupling to bulk phonon modes in clear evidence from the vibronic spectrum. Its value of 2.48 at 77 K results in about 12% of the emitted photons entering the 532 nm ZPL, about three times higher than is the case for NV$^-$. With a total photon count rate 2.8 times that of a single NV centre as noted above, the rate at which ZPL photons are detected is larger by about a factor of eight. In both cases these total count rates appear to be limited by the presence of long-lived metastable states coupled to the optically excited state [33]. In addition, it is unclear from our results as to whether the short fluorescence lifetime of 3.3 ns indicates a strong transition dipole or whether it is the result of non-radiative relaxation, and so the quantum yield may be substantially less than unity.

5. Conclusions

We have identified single-photon emission from a colour centre in high-purity CVD diamond with a strong ZPL at 532 nm. Photon correlation data suggest an electronic system with at least one metastable state accessed from the optically excited state. The centre shows vibronic properties, with a Huang–Rhys factor 2.48 at 77 K. It provides an attractive possibility for use as a single-photon source in the green region of the spectrum.

Acknowledgments

IOP Institute of Physics ⬧ DEUTSCHE PHYSIKALISCHE GESELLSCHAFT

References

[1] Zaitsev A M 2001 *Optical Properties of Diamond* (Berlin: Springer)
[2] Kurtsiefer C, Mayer S, Zarda P and Weinfurter H 2000 *Phys. Rev. Lett.* **85** 290
[3] Gurudev M V, Dutt Childress L, Jiang L, Togan E, Maze J, Jelezko F, Zibrov A S, Hemmer P R and Lukin M D 2007 *Science* **316** 1312
[4] Togan E *et al* 2010 *Nature* **466** 730
[5] Balasubramanian G *et al* 2009 *Nat. Phys.* **8** 283
[6] Benjamin S C, Lovett B W and Smith J M 2009 *Laser Photonics Rev.* **3** 556
[7] Ladd T D, Jelezko F, Laflamme R, Nakamura Y, Monroe C and O'Brien J L 2010 *Nature* **464** 45
[8] Su C-H, Greentree A D and Hollenberg L C L 2008 *Opt. Express* **16** 6240
[9] Wolters J, Schell A W, Kewes G, Nüsse N, Schoengen M, Döscher H, Hannappel T, Löchel B, Barth M and Benson O 2010 *Appl. Phys. Lett.* **97** 141108
[10] Wang C L, Kurtsiefer C, Weinfurter H and Burchard B 2006 *J. Phys. B: At. Mol. Opt. Phys.* **39** 37
[11] Neu E, Steinmetz D, Riedrich-Möller J, Gsell S, Fischer M, Schreck M and Becher C 2011 *New J. Phys.* **13** 025012
[12] Gaebel T, Popa I, Gruber A, Domhan M, Jelezko F and Wrachtrup J 2004 *New J. Phys.* **6** 98
[13] Rabeau J R, Chin Y L, Prawer S, Jelezko F, Gaebel T and Wrachtrup J 2005 *Appl. Phys. Lett.* **86** 131926
[14] Aharonovich I, Castelletto S, Simpson D A, Greentree A D and Prawer S 2010 *Phys. Rev.* A **81** 043813
[15] Aharonovich I, Castelletto S, Johnson B C, McCallum J C, Simpson D A, Greentree A D and Prawer S 2010 *Phys. Rev.* B **81** 121201R
[16] Simpson D A, Ampem-Lassen E, Gibson B C, Trpkovski S, Hossain F M, Huntington S T, Greentree A D, Hollenberg L C L and Prawer S 2009 *Appl. Phys. Lett.* **94** 203107
[17] Khong Y L and Collins A T 1993 *Diam. Relat. Mater.* **2** 1
[18] Khong Y L, Collins A T and Allers L *Diam. Relat. Mater.* **3** 1023
[19] Burton N C, Steeds J W, Meaden G M, Shreter Y G and Butler J E 1995 *Diam. Relat. Mater.* **4** 1222
[20] Kanda H, Watanabe K, Koizumi S and Teraji T *Diam. Relat. Mater.* **12** 20
[21] Kanda H, Watanabe K, Eun K Y and Lee J K 2003 *Diam. Relat. Mater.* **12** 1760
[22] Tallaire A, Collins A T, Charles D, Acharda J, Sussmann R, Gicquela A, Newton M E, Edmonds A M and Cruddace R J 2006 *Diam. Relat. Mater.* **15** 1700
[23] Balmer R S *et al* 2009 *J. Phys.: Condens. Matter* **21** 364221
[24] Grazioso F, Patton B R and Smith J M 2010 *Rev. Sci. Instrum.* **81** 093705
[25] Grazioso F 2010 *PhD Thesis* University of Oxford
[26] Davies G 1981 *Rep. Prog. Phys.* **44** 787
[27] Wehner R, Honk H, Kress W, Goodwin A R and Smith S D 1967 *Solid State Commun.* **5** 307
[28] Zaitsev A M 2000 *Phys. Rev.* B **61** 12909
[29] Lin-Chung P J 1994 *Phys. Rev.* B **50** 16905
[30] Khan R 2010 private communication
[31] Collins A T 2010 private communication
[32] Fourkas J T 2001 *Opt. Lett.* **26** 211
[33] Jelezko F and Wrachtrup J 2006 *Phys. Status Solidi* **203** 3207